A Product Yield Study of the Reaction of HO_2 Radicals with Ethyl Peroxy ($C_2H_5O_2$), Acetyl Peroxy ($CH_3C(O)O_2$), and Acetonyl Peroxy ($CH_3C(O)CH_2O_2$) Radicals

Alam S. Hasson,*,† Geoffrey S. Tyndall,‡ and John J. Orlando‡

Department of Chemistry, California State University, Fresno, California, and Atmospheric Chemistry Division, National Center for Atmospheric Research, Boulder, Colorado

Received: March 14, 2004; In Final Form: May 8, 2004

The reaction between HO_2 and RO_2 radicals represents an important chemical sink for HO_x radicals in the atmosphere. On the basis of a few product yield studies, these reactions are believed to form hydroperoxides almost exclusively (R8a), although several different reaction channels may be thermodynamically accessible (R8a−d): $RO_2 + HO_2 \rightarrow ROOH + O_2$ (R8a); $RO_2 + HO_2 \rightarrow ROH + O_3$ (R8b); $RO_2 + HO_2 \rightarrow RO + OH + O_2$ (R8c); and $RO_2 + HO_2 \rightarrow R'CHO + H_2O + O_2$ (R8d). Branching ratios for reaction R8 were measured for three organic peroxy radicals: ethyl peroxy ($C_2H_5O_2$), acetyl peroxy ($CH_3C(O)O_2$), and acetonyl peroxy ($CH_3C(O)CH_2O_2$) radicals. Product yields were measured using a combination of long-path Fourier transform infrared spectroscopy and high-performance liquid chromatography with fluorescence detection. Measured branching ratios for the reaction of the three organic peroxy radicals with HO_2 are as follows: ethyl peroxy, $Y_{8a-ETH} > 0.93 \pm 0.10$, $Y_{8b-ETH} = Y_{8c-ETH} = Y_{8d-ETH} = 0$; acetyl peroxy, $Y_{8a-ACT} = 0.40 \pm 0.16$, $Y_{8b-ACT} = 0.20 \pm 0.08$, $Y_{8c-ACT} = 0.40 \pm 0.16$, and $Y_{8d-ACT} = 0$; acetonyl peroxy, $Y_{8a-ACN} = 0.33 \pm 0.10$, $Y_{8b-ACN} = Y_{8d-ACN} = 0$, and $Y_{8c-ACN} = 0.67 \pm 0.20$. The atmospheric implications of these branching ratios are discussed.

Introduction

In the troposphere, HO_2 and RO_2 radicals are generated in the photochemical oxidation of organic pollutants as shown in the simplified reaction scheme below.[1]

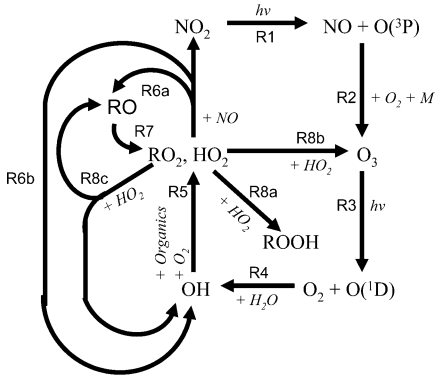

Nitrogen dioxide (NO_2) photolyzes (R1) to form oxygen atoms which combine with oxygen molecules to form ozone (O_3, R2). In turn, O_3 photolyzes, producing electronically excited oxygen atoms (R3) that may then react with water to form hydroxy radicals (OH, R4). These radicals then react with organic pollutants present in the atmosphere, initiating a complex sequence of reactions (R5) that leads to the formation of organic peroxy radicals (RO_2) and hydroperoxy radicals (HO_2).[2] In urban and rural regions, where the concentration of nitrogen oxides ($NO_x = NO + NO_2$) is high, the majority of these species react with nitric oxide (NO) to regenerate NO_2 and form a combination of alkoxy radicals (RO) and OH (R6). These species may generate additional NO_2 because the products of reaction R6 may reform RO_2 and HO_2 via reactions R5 and R7. Thus, the sequence of reactions R1−R7 leads to a buildup of ozone because the yield of NO_2 from this cycle is greater than unity.

The reaction between HO_2 and RO_2 (R8) represents an important sink for radicals in the troposphere. The products of this reaction depend on the chemical identity of the R-group, but on the basis of a limited number of studies of small alkyl peroxy radicals, the major product is thought to be an organic hydroperoxide (R8a)[3−8]

$$RO_2 + HO_2 \rightarrow ROOH + O_2 \qquad \text{(R8a)}$$

Since organic hydroperoxides have lifetimes of 1 day or more,[9] the reaction is a sink for HO_x radicals and thus serves to moderate the oxidizing capacity of the troposphere. The hydroperoxides formed are often soluble in water[10] and may be taken up into cloud and fog droplets, as well as aqueous aerosols. Here, they may play a role in S(IV) to S(VI) conversion,[9] as well as the toxicity of submicron aerosol particles.[11,12]

For more complex organic peroxy radicals, additional product channels for the reaction between RO_2 and HO_2 may exist. Acetyl peroxy radicals ($R = CH_3C(O)-$) are formed in the initial stages of the oxidation of a variety of important atmospheric pollutants including acetaldehyde, acetone, and several internal alkenes. They may also be formed in the troposphere from the oxidation products of many primary organic pollutants, such as isoprene and propene. These peroxy radicals react with HO_2 radicals to form peracetic acid (PAA) via R8a-ACT, as well as acetic acid and ozone (R8b-ACT).[13−17]

$$CH_3C(O)O_2 + HO_2 \rightarrow CH_3C(O)OOH + O_2 \quad \text{(R8a-ACT)}$$

$$CH_3C(O)O_2 + HO_2 \rightarrow CH_3C(O)OH + O_3 \quad \text{(R8b-ACT)}$$

* Address correspondence to this author. E-mail: ahasson@csufresno.edu.
† California State University.
‡ National Center for Atmospheric Research.

10.1021/jp048873t CCC: $27.50
Published on Web 06/22/2004

This reaction represents one of the few known sources of acetic acid in the atmosphere. There have been five previous studies of the branching ratios in this reaction. Niki et al.,[13] Moortgat et al.,[14] Tomas et al.,[17] and Horie and Moortgat[15] all report ratios of R8a-ACT:R8b-ACT of about 0.75:0.25. Moortgat et al. and Tomas et al. both obtained their branching ratios by fitting a kinetic model to experimentally measured concentrations of peroxy radicals in a flash photolysis experiment. Horie and Moortgat determined the branching ratios using yields of ozone and peracetic acid obtained in a Fourier transform infrared (FTIR)/matrix isolation study. In the work by Niki et al., product yields from the Cl-atom-initiated oxidation of $CH_3CHO/HCHO/O_2$ mixtures were measured by FTIR. In these experiments, acetyl peroxy radicals were generated in the reaction between Cl atoms and acetaldehyde (R10):

$$Cl_2 + h\nu \rightarrow 2Cl \quad \text{(R9)}$$

$$Cl + CH_3CHO\ (+O_2) \rightarrow CH_3C(O)O_2 + HCl \quad \text{(R10)}$$

HO_2 radicals were formed in the corresponding reaction between Cl atoms and formaldehyde (R11a):

$$Cl + CH_2O\ (+ O_2) \rightarrow HO_2 + CO + HCl \quad \text{(R11a)}$$

In the presence of large quantities of formaldehyde, essentially all of the acetyl peroxy radicals react with HO_2, and thus the observed product distribution can be used to infer branching ratios in reaction R8. However, in the study by Niki et al. under conditions where acetyl peroxy radicals should react almost exclusively with HO_2, the products from reactions R8a and R8b only account for about 50% of the total carbon balance. More recently, Crawford and co-workers[16] remeasured these branching ratios using a similar technique, using methanol (via reaction R11b) as the HO_2 source

$$Cl + CH_3OH\ (+ O_2) \rightarrow HO_2 + CH_2O + HCl \quad \text{(R11b)}$$

and obtained $Y_{R8a-ACT}:Y_{R8b-ACT} = 0.9:0.1$. In their study, they report that the products from R8a and R8b account for 100% of the reaction products. However, recent work by Orlando and co-workers[18] has shown that the infrared absorption cross section used by Crawford et al. for peracetic acid was too low by a factor of 3. Using the corrected cross section gives branching ratios for R8a-ACT and R8b-ACT that are essentially identical to those obtained by Niki and co-workers.[13] The available literature data thus indicate that there is at least one "missing" product channel for the reaction between $CH_3C(O)O_2$ and HO_2 that accounts for about half of the reaction products. On the basis of its thermochemistry,[19] it is possible that this channel might result in the formation of acetoxy radicals and OH:

$$CH_3C(O)O_2 + HO_2 \rightarrow CH_3C(O)O + OH + O_2 \quad \text{(R8c-ACT)}$$

The formation of OH and an alkoxy radical in the $RO_2 + HO_2$ reaction has recently been observed by Wallington and co-workers[20] in their study of the atmospheric oxidation of C_2F_5-CHO. In this work, the authors report branching ratios for the $C_2F_5C(O)O_2 + HO_2$ reaction to be 0.24 and 0.76 for reaction channels R8b and R8c, respectively.

Reaction R8c is endothermic for R=alkyl, but in the acetyl peroxy radicals, formation of the acetoxy radical + OH + O_2 is almost thermoneutral[21] ($\Delta H = +2$ kcal/mol). The resultant alkoxy radical may then decompose to form carbon dioxide and a methyl radical in a strongly exothermic reaction:

$$CH_3C(O)O \rightarrow CH_3 + CO_2 \quad \text{(R12)}$$

In the presence of excess HO_2, the methyl radicals generated in R12 would form methyl hydroperoxide (MHP, R13).

$$CH_3 + O_2 \rightarrow CH_3O_2 \quad \text{(R13)}$$

$$CH_3O_2 + HO_2 \rightarrow CH_3OOH + O_2 \quad \text{(R14)}$$

Thermochemical considerations indicate that reaction R8c may also occur for acetonyl peroxy radicals ($CH_3C(O)CH_2O_2$).[19]

$$CH_3C(O)CH_2O_2 + HO_2 \rightarrow CH_3C(O)CH_2O + OH + O_2 \quad \text{(R8c-ACN)}$$

The acetonoxy radicals formed in reaction R8c-ACN will then decompose to form acetyl radicals and formaldehyde (R15).

$$CH_3C(O)CH_2O \rightarrow CH_3C(O) + CH_2O \quad \text{(R15)}$$

In the atmosphere, the resultant acetyl radicals would react with O_2 to form $CH_3C(O)O_2$.

While both R8c-ACN and R15 are endothermic, the combination of these two reactions results in an increase in the number of molecules and therefore makes this process entropically favorable and results in $\Delta G_{R8c-ACT} < 0$. In contrast, ΔG_{R8c} for most alkyl peroxy radicals is positive; thus, R8c is thermodynamically allowed for acetonyl peroxy radicals but is not expected to occur for alkyl peroxy radicals. Branching ratios for these reactions, however, have not been measured previously.

An additional reaction channel for the $RO_2 + HO_2$ reactions studied here may also exist. Wallington et al.[22−24] have carried out a series of studies on the branching ratios of $X-CH_2O_2 + HO_2$ reactions (where X = Cl, F, and CH_3O) in which they report the formation of a carbonyl compound and water as a major product channel (R8d):

$$X-CH_2O_2 + HO_2 \rightarrow X\text{-}CHO + H_2O + O_2 \quad \text{(R8d)}$$

The authors measured branching ratios for R8d ranging from 0.40 (X = CH_3O) to 0.73 (X = Cl). Elrod and co-workers[8] have also measured nonnegligible product yields from R8d for the $CH_3O_2 + HO_2$ reaction. The branching ratio increased from 0.11 at 298 K to 0.30 at 218 K, although their room-temperature product yields are somewhat different from other literature values.[19]

If reaction R8c does occur, it may have a significant impact on the chemistry of the troposphere because it leads to less HO_x radical loss and may result in higher predictions of ozone concentrations in tropospheric photochemical simulations. In this work, branching ratios for reactions R8a−c have been measured for ethyl peroxy ($CH_3CH_2O_2$), acetyl peroxy ($CH_3C(O)O_2$), and acetonyl peroxy ($CH_3C(O)CH_2O_2$) radicals. A combination of FTIR and high-performance liquid chromatography (HPLC) was used to obtain product yields for the hydroperoxides formed. Evidence is provided for the existence of reaction channel R8c for both acetyl peroxy and acetonyl peroxy radicals, and implications for the chemistry of the lower atmosphere are considered.

Experimental Section

Branching ratios for reaction R8 were determined by photolyzing mixtures of synthetic air, an organic peroxy radical precursor (ORP), methanol, and Cl_2 in a smog chamber. Cl atoms were generated by exposing the gas mixture to ultraviolet light (R9). These radicals then reacted with the ORP to generate

the peroxy radical of interest. The ORPs for ethyl peroxy, acetyl peroxy, and acetonyl peroxy radicals were ethane, acetaldehyde, and acetone, respectively. The concentration of HO_2 in the experiments was adjusted by adding different concentrations of methanol to the initial reaction mixture. The methanol present reacts with the Cl atoms to form HO_2 in reaction R11b. Initial concentrations of ORPs were in the range $(0.7-1.4) \times 10^{15}$ molecules cm^{-3}, and the ratio of $[CH_3OH]_0$:$[ORP]_0$ was varied between 0 and 5. Some experiments were also carried out using $^{13}CH_3OH$ to produce HO_2. All experiments were performed at a total pressure of 800 Torr, 298 K, and with $[Cl_2]_0 = 3 \times 10^{15}$ molecules cm^{-3}.

Chemical reactions were initiated using radiation in the wavelength range 235−400 nm, which was generated by filtering light from a xenon arc lamp. Changes in the concentrations of reactants and products were monitored by FTIR spectroscopy and HPLC with fluorescence detection (HPLC−fluorescence), as described in detail previously.[25−27] All experiments were performed in a 47 L stainless steel chamber coupled to a Bomem DA3.01 FTIR spectrometer via Hanst type optics, providing a path length of 32.6 m. IR spectra were collected at a resolution of 1 cm^{-1} by averaging 200 scans in the wavelength range 800−3900 cm^{-1}.

Gas-phase hydroperoxides formed within the chamber were extracted into the aqueous phase for analysis by HPLC−fluorescence using a helical coil collector.[28] The coil collector was connected to a sampling port on the chamber via approximately 5 m of 1/8 in. Teflon tubing. Samples were removed at a flow rate of 250 mL min^{-1} and were diluted in a 2 L min^{-1} flow of zero grade N_2 before introduction into the coil. Flow rates were determined using both Dri-Cal flowmeters and by monitoring pressure changes within the chamber. The volume of each sample removed from the cell constituted less than 1% of its total volume. Water-soluble compounds present in the sample were extracted into a stripping solution consisting of 1×10^{-3} M sulfuric acid and 1×10^{-4} M Na_2EDTA within the stripping coil. The stripping solution was passed through the coil at 0.6 mL min^{-1} using a peristaltic pump. At the end of the coil, the stripping solution containing the dissolved hydroperoxides was collected for analysis by HPLC. Hydroperoxides are first separated using a reversed-phase C-18 HPLC column. At the end of the column, a "fluorescence reagent" containing the reagents horseradish peroxidase and *para*-hydroxyphenyl acetic acid (POHPAA) are added. The horseradish peroxidase enzyme catalyses the stoichiometric reaction between hydroperoxides and POHPAA resulting in the formation of one POHPAA dimer for every hydroperoxide molecule present. This dimer is detected by fluorescence, with excitation and emission wavelengths of 320 and 400 nm, respectively. The hydroperoxides are identified by comparison of their retention times with those of hydroperoxide samples synthesized in the laboratory. The concentrations of hydroperoxides are determined by comparison of the integrated fluorescence peak areas with those of standardized hydrogen peroxide solutions.

Preliminary work indicated that both photolysis and wall loss of the ORP and products were negligible on the time scale of the experiments. In the initial stages of the study, an intercomparison of the HPLC and FTIR techniques for hydroperoxide analysis was performed. Peracetic acid was introduced into the chamber in the concentration range $(0.5-4.5) \times 10^{14}$ molecules cm^{-3} by injecting known volumes of a calibrated peracetic acid solution into the evacuated chamber. Nitrogen was then introduced into the chamber to make up the total pressure to 800 Torr. Concentrations measured using the two techniques were then compared to the actual concentrations present, as shown in Figure 1. The experiments demonstrate that the two techniques measure concentrations that are indistinguishable from each other and that they are within the experimental uncertainties of the true concentration. The FTIR concentrations were obtained using the peracetic acid absorption cross section of 5.3×10^{-19} cm^2 $molecule^{-1}$ at 1295 cm^{-1} reported by Orlando and co-workers.[18] The excellent agreement with the HPLC technique justifies the use of this value for the absorption cross section rather than the much lower cross section reported by Crawford et al.[16]

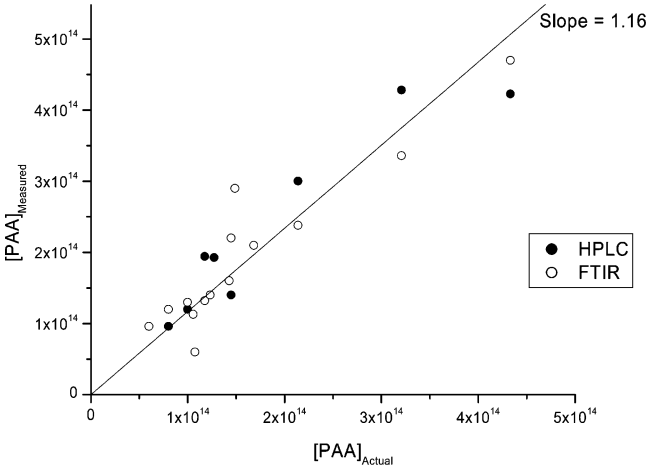

Figure 1. Comparison of PAA concentrations measured by HPLC and FTIR.

TABLE 1: Product Yields from the Photooxidation of Methanol/Ethane/Cl_2 Mixtures

	yield/%		
	HPLC	FTIR	
$[CH_3OH]_0/[C_2H_6]_0$	EHP	EHP	CH_3CHO
0	35	35	47
1	88	106	0
2	94	83	0
3	95	95	9
5	93	84	12

Results and Discussion

(i) Ethyl Peroxy + HO_2. Measured product yields (defined as Δ[product]/ $-\Delta$[reactant]) in the photooxidation of C_2H_6/CH_3OH/Cl_2/O_2 mixtures are shown in Table 1 and Figure 2. In the absence of methanol, yields of acetaldehyde and ethyl hydroperoxide were 47% and 35%, respectively. These data are in good agreement with previous measurements.[29,30] In the presence of equal concentrations of ethane and methanol, the acetaldehyde yield drops to zero, and the EHP yield rises to 93%. Within the experimental uncertainties, the yields of these products remain constant as the initial concentration of methanol increases from this value. In all of the experiments where methanol was present, the product yield plots for acetaldehyde (not shown) are curved upward indicating that this compound is not a primary product.

As described above, ethyl peroxy radicals are generated in the reaction of ethane with Cl atoms followed by O_2 addition:

$$C_2H_6 + Cl\ (+ O_2) \rightarrow CH_3CH_2O_2 + HCl \qquad (R16)$$

These peroxy radicals then undergo self-reaction to form ethoxy radicals (R17a), which react with O_2 to form acetaldehyde and HO_2, or molecular products (R17b).

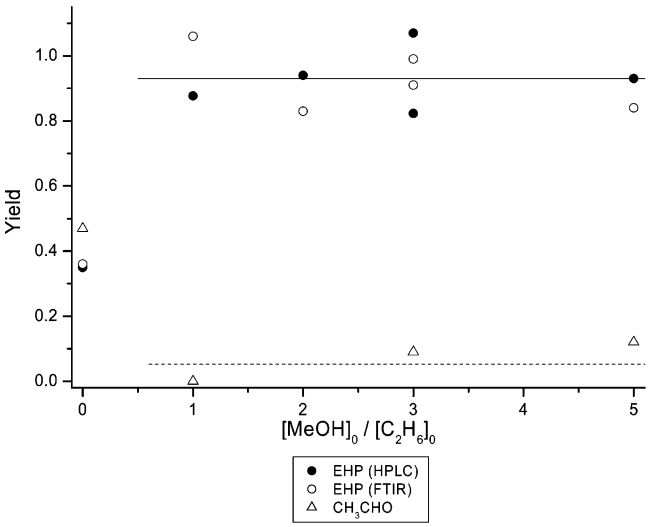

Figure 2. Product yields from the chlorine-atom-initiated oxidation of ethane/methanol mixtures.

$$2CH_3CH_2O_2 \rightarrow 2CH_3CH_2O + O_2 \quad \text{(R17a)}$$

$$\rightarrow CH_3CHO + CH_3CH_2OH + O_2 \quad \text{(R17b)}$$

$$CH_3CH_2O + O_2 \rightarrow CH_3CHO + HO_2 \quad \text{(R18)}$$

The HO_2 radicals generated here may also react with ethyl peroxy radicals resulting in the formation of EHP.

$$CH_3CH_2O_2 + HO_2 \rightarrow CH_3CH_2OOH + O_2 \quad \text{(R8a-ETH)}$$

$$\rightarrow \text{other products} \quad \text{(R8b-ETH)}$$

The competition between reactions R17 and R8-ETH accounts for the observed product distribution in experiments performed in the absence of methanol (e.g., refs 29 and 30).

In the presence of methanol, HO_2 radicals are also generated in reaction R11, and the rate of reaction R8-ETH increases relative to R17. Because k_{16} is ~100 times smaller than $k_{8\text{-ETH}}$,[31] reaction R8-ETH accounts for essentially 100% of the reaction products in experiments where $[CH_3OH]_0$:$[C_2H_6]_0 > 1$, and the product distribution is independent of the initial concentrations of reactants. Under these conditions, the average yield of ethyl hydroperoxide is 0.93, indicating that R8a-ETH is the dominant product channel for the reaction between ethyl peroxy radicals and HO_2. This result is consistent with previous studies of reaction R8-ETH, as shown in Table 2. The small concentrations of acetaldehyde in these experiments can be accounted for by the reaction of EHP with Cl atoms

$$CH_3CH_2OOH + Cl \rightarrow CH_3CHOOH + HCl \quad \text{(R19)}$$

$$CH_3CHOOH \rightarrow CH_3CHO + OH \quad \text{(R20)}$$

(ii) Acetyl Peroxy + HO_2. This reaction was studied using the photolysis of $CH_3CHO/CH_3OH/Cl_2/O_2$ mixtures. Typical changes in the concentrations of acetaldehyde and the reaction products during an experiment are shown in Figure 3. Product yields of methyl hydroperoxide (MHP), peracetic acid (PAA), acetic acid, and CO_2 observed for various $[CH_3OH]/[CH_3CHO]$ ratios (determined from the slope of product yield plots such as the one shown in Figure 3) are shown in Table 3 and Figure 4. As the $[CH_3OH]_0$:$[CH_3CHO]_0$ ratio increases, the yields of MHP, PAA, and acetic acid rise from 17%, 12%, and 6%, respectively, at a $[CH_3OH]_0$:$[CH_3CHO]_0$ ratio of 0, to 42%, 30%, and 13%, respectively, at a ratio of 5. In contrast, the yield of CO_2 falls from 89% to 51% over the same range. The trend in the data indicate that these yields have not leveled off at the highest $[CH_3OH]_0$:$[CH_3CHO]_0$ ratio investigated and that the yields of these products will be somewhat different at even higher ratios. Because of interference from saturated methanol bands in the IR spectra, however, higher ratios of CH_3OH:CH_3CHO could not be investigated.

TABLE 2: Experimental Branching Ratios Y_{R8a}, Y_{R8b}, and Y_{R8c}

	branching ratios			
reaction	Y_{R8a}	Y_{R8b}	Y_{R8c}	ref
$C_2H_5O_2 + HO_2$	$> 0.93 \pm 0.10$	0	0	this work
	1.02	0	0	4[a]
	1.04	0	0	7[a]
$CH_3C(O)O_2 + HO_2$	0.4 ± 0.16	0.2 ± 0.08	0.4 ± 0.16	this work
	0.34	0.1		13[a]
	0.3	0.1		16[a,b]
$CH_3C(O)CH_2O_2 + HO_2$	0.33 ± 0.10	0	0.67 ± 0.20	this work
	1	0	0	33[c]

[a] Determined from smog chamber product yield experiments using high HO_2 precursor. [b] Branching ratios modified using IR absorption cross section for PAA from ref 18. See text for details. [c] Determined flash-photolysis experiments.

TABLE 3: Product Yields from the Photooxidation of Methanol/Acetaldehyde/Cl_2 Mixtures

	product yield/%					
	HPLC		FTIR			
$[CH_3OH]_0$/$[CH_3CHO]_0$	MHP	PAA	MHP	PAA	acetic acid	CO_2
0	14	9	19	15	6	89
1	26	15	30	23	9	83
1.5	n.m.[a]	n.m.	34	27	10	79
2	42	25	41	37	15	75
3	40	25	36	35	14	90
4	41	25	46	37	12	70
5	n.m.	n.m.	44	32	14	51

[a] n.m = not measured.

As described above, Cl atoms react with acetaldehyde in the presence of O_2 to form acetyl peroxy radicals (R10). The observed PAA and acetic acid are formed almost exclusively in the reaction of acetyl peroxy radicals with HO_2 (R8a-ACT and R8b-ACT, respectively). In the absence of methanol, the concentration of HO_2 is comparatively low and thus yields of these products are also low. Under these conditions, the principal fate of the acetyl peroxy radicals is reaction with itself or with methyl peroxy radicals to form acetoxy radicals.

$$CH_3C(O)O_2 + RO_2 \rightarrow CH_3C(O)O + RO + O_2 \quad \text{(R21)}$$

These radicals then decompose to form CO_2 and methyl radicals via reaction R12, resulting in the high CO_2 yield observed in these experiments. The methyl radicals formed in R12 may then generate MHP in reaction R13.

As the concentration of methanol (and thus HO_2) rises, acetyl peroxy radicals increasingly react with HO_2. In the currently accepted reaction scheme, R8-ACT only proceeds via two pathways (R8a-ACT and R8b-ACT) leading to an increase in the yields of PAA and acetic acid. As the yields of these compounds rise, the yield of acetoxy radicals via R21 decreases, and thus the CO_2 yield (via R12) falls. The trend in the MHP yield is expected to be more complex. As the methanol concentration increases, the yield of methyl radicals decreases, but a greater fraction of these methyl radicals react via R13 to form MHP. At high CH_3OH:CH_3CHO ratios, however, the MHP yield is expected to decrease.

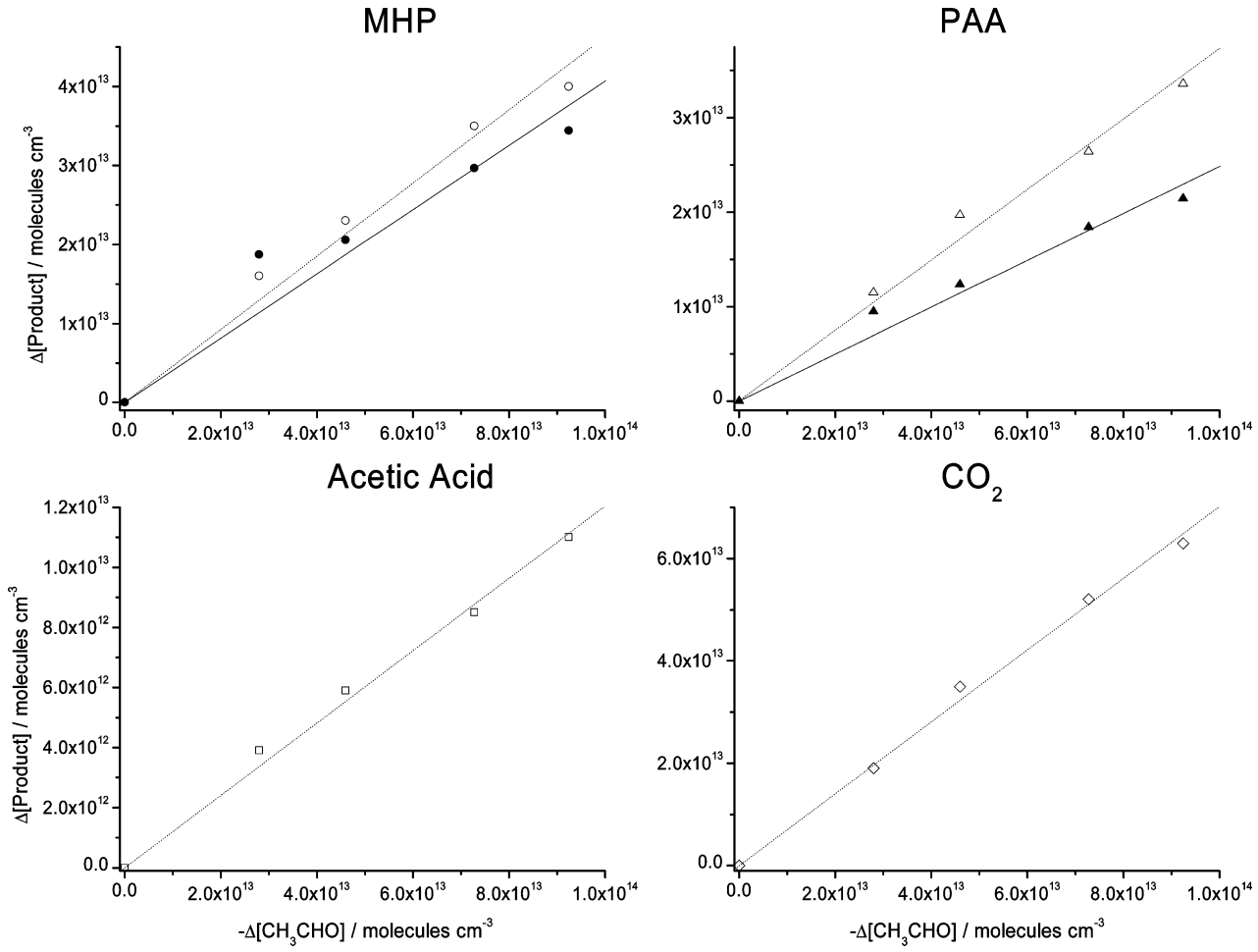

Figure 3. Typical product yield plots from the chlorine-atom-initiated oxidation of an acetaldehyde/methanol mixture ($[CH_3OH]_0/[CH_3CHO]_0 = 4$) Open symbols represent FTIR measurements; filled symbols represent HPLC measurements. Dashed lines are least-squares fits to FTIR data points; solid lines are least-squares fits to HPLC data points.

Inspection of the product yields in Figure 4 reveals two important features at high methanol concentrations. First, the yields of the established product channels from the reaction of acetyl peroxy radicals with HO_2 (R8a-ACT and R8b-ACT) only account for about 50% of the reaction products. Under these conditions, numerical simulations indicate that the combined product yields should be 65% (see below). Second, the yields of CO_2 and MHP decrease far more slowly than expected at these high methanol concentrations. These observations are consistent with a third significant product channel from the reaction of acetyl peroxy radicals with HO_2 that results in the formation of acetoxy radicals. These radicals subsequently react via R12 and R13 to form the observed CO_2 and MHP products, which are observed in excess of levels expected on the basis of the occurrence of R8a-ACT and R8b-ACT alone. These observations thus provide indirect evidence for the occurrence of reaction R8c-ACT in which acetyl peroxy radicals react with HO_2 to form acetoxy radicals and OH radicals.

To better understand the observed product distributions, kinetic modeling was carried out using the Acuchem program.[32] The reaction scheme used in these simulations is shown in Table 4. In this scheme, the overall rate coefficient for the reaction between acetyl peroxy radicals and HO_2 (k_{8-ACT}) and the branching ratios (Y_{8a-ACT}, Y_{8b-ACT}, and Y_{8c-ACT}) were treated as adjustable parameters. A comparison between measured product yields and results obtained in these simulations is shown in Figure 4. Initially, the branching ratio for R8c-ACT (Y_{8c-ACT}) was set to zero and k_{8-ACT} was set to the recommended literature value (1.4×10^{-11} cm^3 molecule^{-1} s^{-1}). Y_{8a-ACT} and Y_{8b-ACT} were set to 0.7, and 0.3, respectively, reflecting the relative yields of the products of these reactions (peracetic acid and acetic acid, respectively). This simulation (simulation 1) fails to capture two of the important experimental observations. First, the model predicts that the MHP yield will decrease slightly as the CH_3OH:CH_3CHO ratio increases from 1 to 5, whereas the MHP yield is actually observed to increase under these conditions. Second, this model predicts that the CO_2 yield will fall from 80% to 40% as the CH_3OH:CH_3CHO ratio increases from 1 to 5. The experimental yields decrease much less dramatically and are 15−20% higher than the predicted yields at any given $[CH_3OH]_0$:$[CH_3CHO]_0$ ratio. The branching ratios used in simulation 1 are slightly different from the literature recommendation for these reactions,[19] but this small difference cannot account for the difference between the predicted and experimental product yields.

In a second set of simulations, the impact of Y_{8c-ACT} on the product yields was investigated. The best fit to the experimental data was obtained for values of Y_{8a-ACT}, Y_{8b-ACT}, and Y_{8c-ACT} of 0.5, 0.2, and 0.3, as shown in Figure 4. Because of the fairly large uncertainties in the experimental product yields, we estimate the uncertainties in the branching ratios to be about 40%. Nonetheless, the simulations demonstrate that by including reaction channel R8c-ACT in the reaction scheme, the discrepancies between the measured and simulated yields of MHP and CO_2 disappear. The data previously obtained by Niki and coworkers,[13] and by Crawford et al.[16] (corrected using Orlando

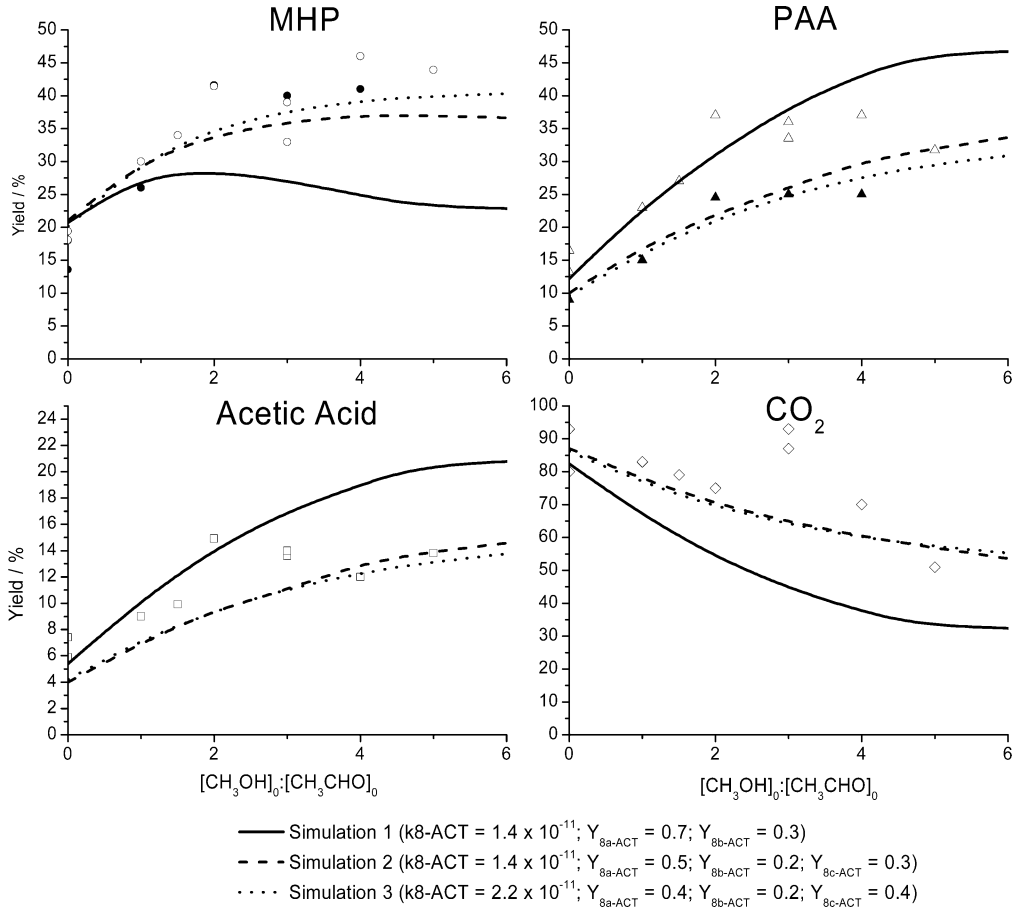

Figure 4. Comparison of experimental and model product yields from the chlorine-atom-initiated oxidation of acetaldehyde/methanol mixtures (see text for details). Open symbols represent FTIR measurements; filled symbols represent HPLC measurements.

et al.'s PAA absorption cross section[18]), are also modeled well by these simulations.

In a recent study,[16] the rate constant k_{8-ACT} was reported to be about 3 times higher than the accepted literature value. To investigate the potential impact of the uncertainty in this rate coefficient on the product distribution, a third set of simulations was carried out in which the sum of $k_{8a-ACT} + k_{8b-ACT}$ was fixed at 1.4×10^{-11} cm^3 molecule^{-1} s^{-1}, while the branching ratios of reaction R8-ACT and the overall rate coefficient (k_{8a-ACT}) were allowed to vary. The best agreement with experimental data (shown in Figure 4, simulation 3) was obtained with $Y_{8a-ACT} = 0.4$, $Y_{8b-ACT} = 0.2$, and $Y_{8c-ACT} = 0.4$, corresponding to an overall rate constant for R8-ACT of 2.2×10^{-11} cm^3 molecule s^{-1}. It is clear from Figure 4 that the optimized results from simulations 2 and 3 are experimentally indistinguishable, and thus these experiments cannot be used to resolve the discrepancy in k_{8-ACT}. Further, it can be seen that any uncertainty in k_{8-ACT} translates into uncertainties in the branching ratios of R8-ACT. Nonetheless, it is apparent that regardless of the true value for k_8-ACT, a large branching ratio is required for R8c-ACT to obtain a good fit to the experimental data. The results from simulation 3 fit the experimental data slightly better than simulation 2; hence, the recommended branching ratios for the reaction are $Y_{8a-ACT} = 0.40 \pm 0.16$, $Y_{8b-ACT} = 0.20 \pm 0.08$, and $Y_{8c-ACT} = 0.40 \pm 0.16$. The large errors reported here reflect the uncertainty in k_8-ACT.

It is well established[17] that HO_2 radicals react with carbonyl compounds to form a hydroxy peroxy radical that may then subsequently react to form some of the observed products.

$$CH_3CHO + HO_2 (+ M) \leftrightarrow CH_3CH(OH)OO \quad (R22)$$

It is apparent from these simulations, however, that under all experimental conditions investigated the equilibrium in R22 lies well to the left and that this chemistry cannot account for the discrepancies between the expected and observed product distributions.

As described in the Introduction section, previous studies of reaction R8-ACT did not consider reaction R8c-ACT in the determination of the branching ratios. Nonetheless, the three previous product yield studies of this reaction[13,15,16] are consistent with the corresponding branching ratios reported here because a significant fraction of the total carbon balance was not accounted for by R8a-ACT and R8b-ACT. Branching ratios for these previous studies are given in Table 2. Studies in which absolute yields of organic acids were not reported[14,15] are not included in this table. The yield of PAA in the Crawford et al. study[16] has been corrected using the IR absorption cross section of Orlando et al.,[18] as discussed above. Studies which measured O_3 fit our yields better than previous determinations of the acetic acid yield.

Crawford et al.[16] followed the temporal evolution of peroxy radical concentrations from the acetyl peroxy + HO_2 reaction by flash photolysis. By using a reaction mechanism incorporating channels R8a-ACT and R8b-ACT, numerical simulations underestimate the CH_3O_2 concentration by roughly a factor of 2 (figure 4 in ref 16). To test whether channel R8c can explain this discrepancy, numerical simulations were conducted under the appropriate experimental conditions. Incorporation of channel R8c-ACT into the mechanism leads to much better agreement of the model with the experimental data, providing further indirect evidence for this reaction pathway. It is possible that flash photolysis experiments were "blind" to the OH-producing

TABLE 4: Reaction Scheme Used in Kinetic Modeling of Acetaldehyde and Acetone Chemistry

reaction[a]	rate coefficient/s^{-1} or cm^3 $molecule^{-1}$ s^{-1} [b]
$Cl_2 = Cl+Cl$ (R9)	1×10^{-4}
Cl + $CH_3C(O)CH_3$ = **$CH_3C(O)CH_2$ + HCl (R23)**	2.1×10^{-12}
$CH_3C(O)CH_2 + O_2 = CH_3C(O)CH_2O_2$ (R23)	5×10^{-12}
$2CH_3C(O)CH_2O_2 = 2CH_3C(O)CH_2O + O_2$	6×10^{-12}
$2CH_3C(O)CH_2O_2 = CH_3C(O)CHO + CH_3C(O)CH_2OH + O_2$	2×10^{-12}
$CH_3C(O)CH_2O = CH_3C(O)O_2 + CH_2O$ (R15)	6×10^{7}
$CH_3C(O)CH_2O + O_2 = HO_2 + CH_3C(O)CHO$	1×10^{-14}
$CH_3C(O)CH_2O_2 + CH_3C(O)O_2 = CH_3C(O)CH_2O + CH_3CO_2 + O_2$	1×10^{-11}
$CH_3C(O)CH_2O_2 + CH_3C(O)O_2 = CH_3C(O)CHO + CH_3C(O)OH + O_2$	1×10^{-12}
$CH_3C(O)CH_2O_2 + CH_3O_2 = CH_3C(O)CH_2O + CH_3O + O_2$	1.1×10^{-12}
$CH_3C(O)CH_2O_2 + CH_3O_2 = CH_3C(O)CHO + CH_3OH + O_2$	1.4×10^{-12}
$CH_3C(O)CH_2O_2 + CH_3O_2 = CH_3C(O)CH_2OH + CH_2O + O_2$	1.4×10^{-12}
$CH_3C(O)CH_2O_2 + HO_2 = CH_3C(O)CH_2OOH$ (R8a-ACN)	variable, see text for details
$CH_3C(O)CH_2O_2 + HO_2 = CH_3C(O)CH_2O + OH$ (R8c-ACN)	variable, see text for details
$CH_3C(O)O_2 + CH_3C(O)O_2 = CH_3CO_2 + CH_3CO_2 + O_2$	1.4×10^{-11}
$CH_3C(O)O_2 + CH_3O_2 = CH_3CO_2 + CH_3O + O_2$	1.1×10^{-11}
$CH_3C(O)O_2 +$ **HO_2** $= CH_3C(O)OOH$ **(R8a-ACT)**	variable, see text for details
$CH_3C(O)O_2 +$ **HO_2** $= CH_3C(O)OH +$ **O_3 (R8b-ACT)**	variable, see text for details
$CH_3C(O)O_2 +$ **HO_2** $=$ **$CH_3CO_2 +$ OH (R8c-ACT)**	variable, see text for details
$CH_3O_2 + CH_3O_2 = CH_3OH + CH_2O + O_2$	2.2×10^{-13}
$CH_3O_2 + CH_3O_2 = CH_3O + CH_3O + O_2$	1.3×10^{-13}
$CH_3O_2 + HO_2 = CH_3OOH + O_2$ (R13)	5.2×10^{-12}
$HO_2 + HO_2 = H_2O_2 + O_2$	3×10^{-12}
$CH_3O + O_2 = HO_2 + CH_2O$	2×10^{-15}
$Cl + CH_2O = HCO + HCl$	7.3×10^{-11}
$HCO + O_2 = HO_2 + CO$	5.5×10^{-12}
Cl + **CH_3CHO** $= CH_3C(O)O_2 +$ **HCl (R10)**	8×10^{-11}
CH_3CO_2 $+ O_2 =$ **CH_3O_2** $+$ **CO_2 (R12)**	1×10^{8}
$CH_2O + HO_2 = CH_2(OH)O_2$	1×10^{-13}
$CH_2(OH)O_2 = CH_2O + HO_2$	50
$CH_2(OH)O_2 = HCOOH$	7
$Cl + CH_3O_2 = CH_3O + ClO$	1×10^{-10}
$Cl + CH_3O_2 = CH_2O_2 + ClO$	1×10^{-10}
$Cl + HO_2 = HCl + O_2$	3.2×10^{-11}
$Cl + HO_2 = ClO + OH$	9×10^{-12}
$Cl + CH_3C(O)O_2 = CH_3C(O)O + ClO$	1×10^{-10}
$ClO + HO_2 = HOCl + O_2$	5×10^{-12}
$ClO + CH_3O_2 = Cl + CH_3O + O_2$	1.6×10^{-12}
$ClO + CH_3C(O)O_2 = Cl + CH_3C(O)O + O_2$	3×10^{-12}
$OH + CH_3CHO + O_2 = H_2O + CH_3C(O)O_2$	1.3×10^{-11}
$OH + CH_2O = HCO + H_2O$	1×10^{-11}
$OH + CH_3OH = CH_2OH + H_2O$	9×10^{-13}
$OH + HO_2 = + H_2O + O_2$	1.1×10^{-10}
$Cl + CH_3OH = CH_2OH + HCl$ (R11)	6×10^{-11}
$CH_2OH + O_2 = HO_2 + CH_2O$	9.1×10^{-12}
$Cl + O_2 = ClOO$	5.4×10^{-14}
$ClOO = Cl + O_2$	2×10^{6}
$Cl + ClOO = Cl_2 + O_2$	3×10^{-10}
$Cl + ClOO = ClO + ClO$	1.2×10^{-11}
$Cl + HCOOH (+O_2) = HCl + CO_2 + HO_2$	2×10^{-13}
$Cl + CH_3OOH = HCl + OH + CH_2O$	6×10^{-11}
$Cl + H_2O_2 = HCl + HO_2$	4×10^{-13}
$Cl + CH_3C(O)OH = CH_3C(O)O_2$	5×10^{-15}
$Cl + CH_3C(O)OH = CH_3O_2 + CO_2$	2.5×10^{-14}
$Cl + O_3 = ClO + O_2$	1×10^{-11}
$HO_2 + O_3 = OH + O_2$	2×10^{-15}
$OH + O_3 = HO_2 + O_2$	7×10^{-14}
$OH + CO (+ O_2) = CO_2 + HO_2$	2×10^{-13}
$OH + CH_3C(O)OH (+O_2) = H_2O + CH_3O_2 + CO_2$	8×10^{-13}
$OH + CH_3C(O)OH = H_2O + CH_3C(O)O_2$	8×10^{-13}
$OH + CH_3OOH = H_2O + CH_3O_2$	7×10^{-12}
$OH + H_2O_2 = H_2O + HO_2$	1.7×10^{-12}
$CH_3O_2 + ClO = CH_3OCl + O_2$	6×10^{-13}
$ClO + ClO = Cl_2 + O_2$	5×10^{-15}
$ClO + ClO = Cl + Cl + O_2$	8×10^{-15}
$Cl + CH_3C(O)CHO (+O_2) = HCl + CH_3C(O)O_2 + CO$	4.5×10^{-11}
$Cl + CO = ClCO$	2.6×10^{-14}
$ClCO = Cl + CO$	5×10^{3}
$OH + CH_3C(O)CH_3 = H_2O + CH_3C(O)CH_2$	1.4×10^{-13}
$Cl + CH_3C(O)CH_2O_2 = CH_3C(O)CH_2O + ClO$	1×10^{-10}
$CH_3C(O)CH_2O_2 + ClO = CH_3C(O)CH_2O + Cl + O_2$	1.5×10^{-12}
$CH_3C(O)CH_2O_2 + ClO = CH_3C(O)CH_2OCl + O_2$	5×10^{-13}
$OH + CH_3C(O)CHO (+ O_2) = H_2O + CH_3C(O)O_2 + CO$	1.6×10^{-11}
$Cl + CH_3C(O)CH_2OOH = HCl + OH + CH_3C(O)CHO$	1×10^{-10}
$OH + HCl = H_2O + Cl$	8×10^{-13}
$Cl + CH_3C(O)CH_2OH (+ O_2) = HCl + CH_3C(O)CHO + HO_2$	6×10^{-11}
$OH + CH_3C(O)CH_2OH = H_2O + CH_3C(O)CHO + HO_2$	1.2×10^{-12}
$OH + CH_3C(O)CH_2OOH = H_2O + OH + CH_3C(O)CHO$	5×10^{-12}
$OH + CH_3C(O)CH_2OOH = H_2O + CH_3C(O)CH_2O_2$	5×10^{-12}

[a] Some of the key reactions referred to in the text are highlighted in bold. [b] Rate coefficients are taken from refs 18 and 19.

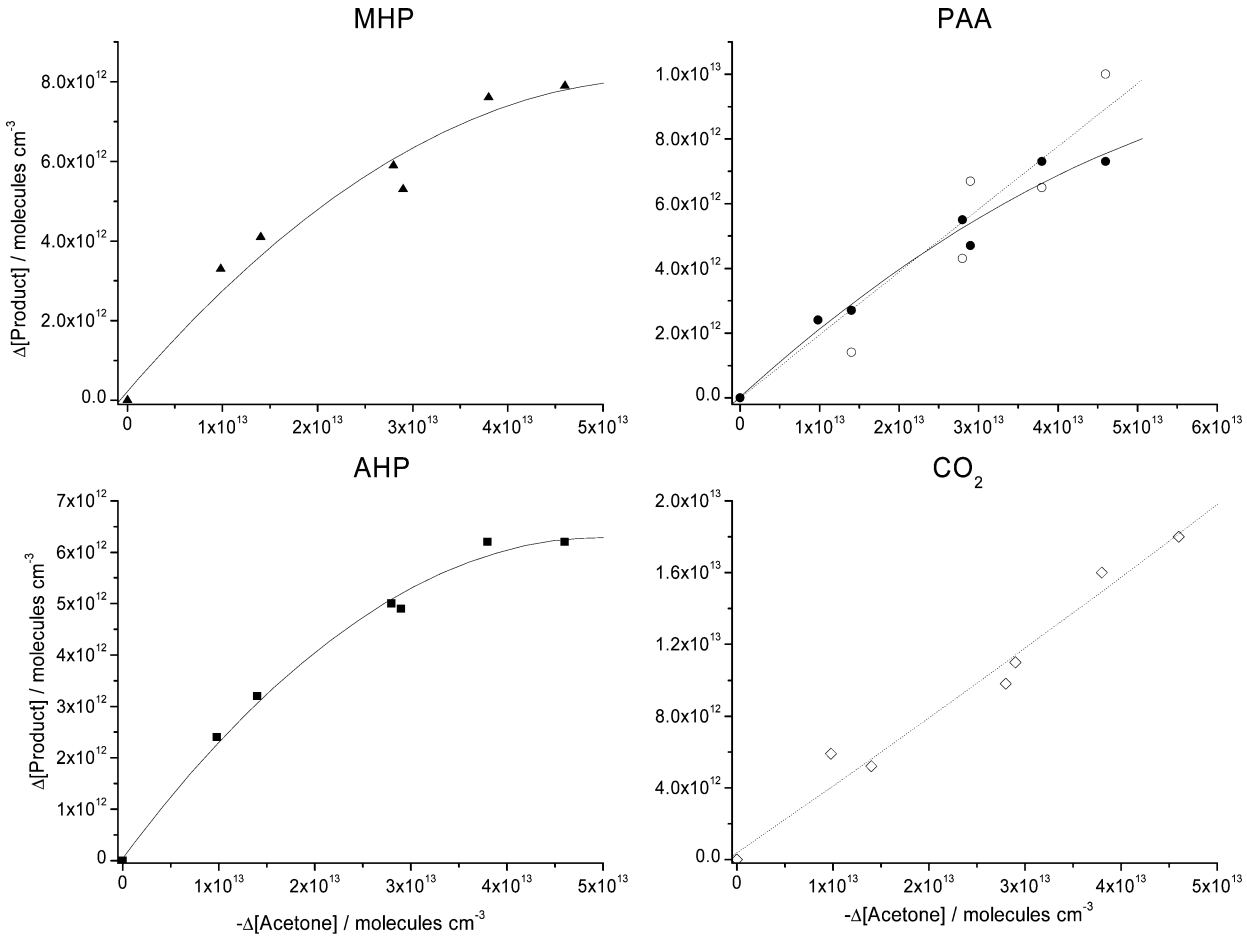

Figure 5. Typical product yield plots from the chlorine-atom-initiated oxidation of an acetone/methanol mixture ($[CH_3OH]_0/[CH_3C(O)CH_3]_0 = 0.5$) Open symbols represent FTIR measurements; filled symbols represent HPLC measurements. Dashed lines are least-squares fits to FTIR data points; solid lines are least-squares fits to HPLC data points.

TABLE 5: Product Yields from the Photooxidation of Methanol/Acetone/Cl_2 Mixtures

	product yields/%						
	HPLC			FTIR			
$[CH_3OH]_0/[CH_3CHO]_0$	MHP	PAA	AHP	PAA	CO_2	CO[a]	CH_2O[a]
0	16	16	13	15	58	n.m.[b]	n.m.
0.125	31	23	27	18	43	n.m.	n.m.
0.25	32	29	30	13	33	40	35
0.5	30	25	28	19	39	n.m.	n.m.

[a] Yields measured in separate experiment using $^{13}CH_3OH$. [b] n.m. = not measured.

channel, since it regenerates radicals. In this case, our branching ratio allows for an overall rate coefficient as high as 2.3×10^{-11} cm^3 $molecule^{-1}$ s^{-1}. However, careful reanalysis of the original data from refs 16 and 17 would be required to confirm this.

(iii) Acetonyl Peroxy + HO_2. Typical changes in the concentrations of acetone and the reaction products following the photolysis of Cl_2/acetone/CH_3OH mixtures in air are shown in Figure 5. As can be seen in this figure, some of the product yield plots are curved because of the reaction of these products with Cl atoms. In such cases, the product yields were determined by fitting a polynomial to the data points and evaluating the slope of the curve at the origin. Product yields of acetonyl hydroperoxide (AHP), PAA, MHP, and CO_2 obtained during the photolysis of $CH_3COCH_3/CH_3OH/Cl_2/O_2$ mixtures are shown in Table 5 and Figure 6. Because of the slow reaction between acetone and Cl atoms,[31] much lower $[CH_3OH]_0$:$[acetone]_0$ ratios are needed to generate an excess of HO_2 radicals, thus the highest ratio used in this work was 0.5. In the absence of methanol, experimental yields of AHP, PAA, and MHP are 13%, 16%, and 16%, respectively. As the concentration of methanol increases, the yields of these hydroperoxides rise to 28%, 21%, and 31%, respectively. In contrast, the yield of CO_2 decreases from 58% to 38% as the $[CH_3OH]_0$:$[acetone]_0$ ratio increases from 0 to 0.5.

In the absence of methanol, Cl atoms react with acetone to form acetonyl peroxy radicals (R23), which then predominantly react with other peroxy radicals present to form acetonoxy radicals (R24a).

$$CH_3C(O)CH_3 + Cl\ (+ O_2) \rightarrow CH_3C(O)CH_2O_2 + HCl \quad \text{(R23)}$$

$$CH_3C(O)CH_2O_2 + RO_2 \rightarrow CH_3C(O)CH_2O + RO + O_2 \quad \text{(R24a)}$$

$$\rightarrow CH_3C(O)CHO + ROH + O_2 \quad \text{(R24b)}$$

$$\rightarrow CH_3C(O)CH_2OH + R'CHO + O_2 \quad \text{(R24b')}$$

These radicals then form formaldehyde and acetyl radicals in reaction R15, which can subsequently produce PAA and MHP as described for the oxidation of acetaldehyde above. A significant amount of HO_2 is formed in secondary chemistry, which may also react with acetonyl peroxy radicals to generate the observed AHP.

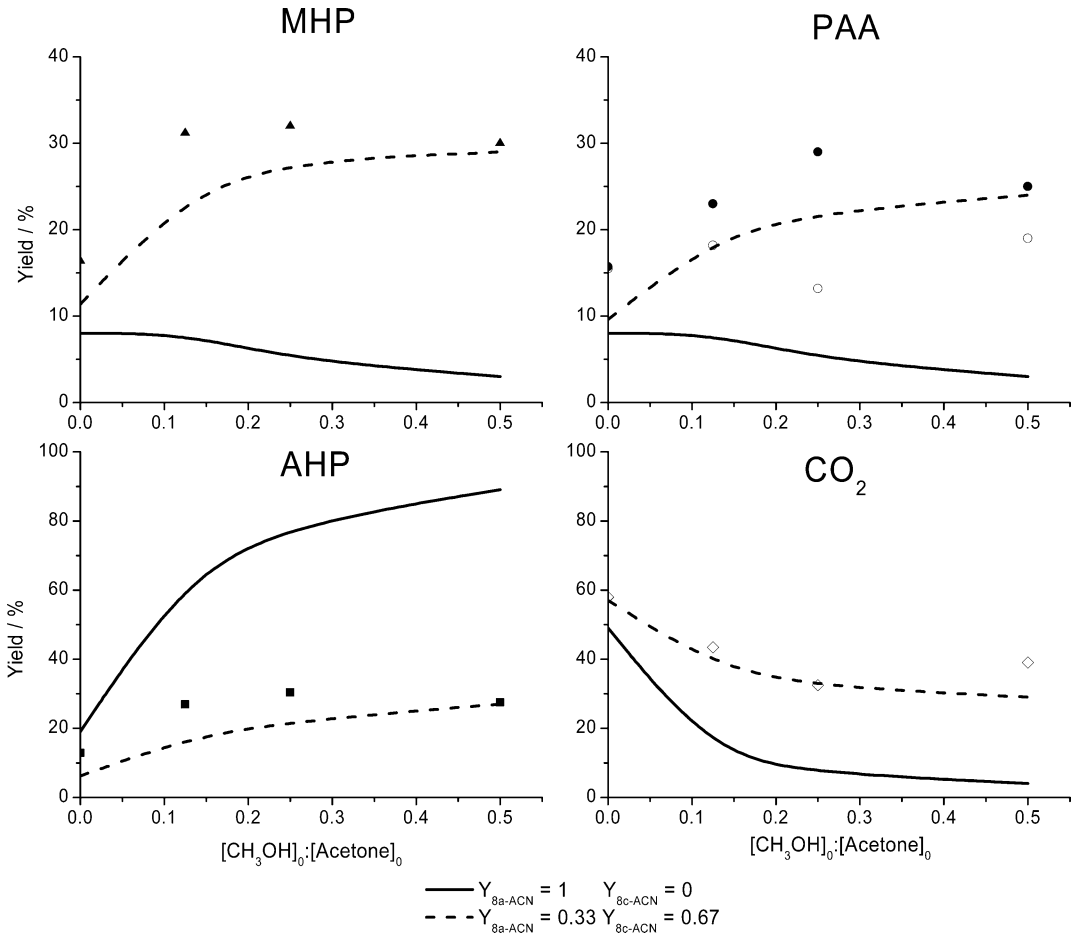

Figure 6. Comparison of experimental and model product yields from the chlorine-atom-initiated oxidation of acetone/methanol mixtures (see text for details). Open symbols represent FTIR measurements; filled symbols represent HPLC measurements

$$CH_3C(O)CH_2OO + HO_2 \rightarrow CH_3C(O)CH_2OOH + O_2 \quad \text{(R8a-ACN)}$$

If reaction R8a-ACN were the only product channel for the acetonyl peroxy + HO_2 reaction, the yield of AHP would rise to unity and the yields of MHP, PAA, and CO_2 would fall to zero as the methanol (and thus the HO_2 concentration) increases. It is clear from Figure 6 that this does not occur and implies that as with the acetyl peroxy + HO_2 reaction, a significant radical channel leading to acetonoxy radicals and OH is occurring with the acetonyl peroxy + HO_2 reaction (R8c-ACN).

To investigate this channel further, simulations were performed using an Acuchem model which incorporated the reactions shown in Table 4. Results of these simulations are shown in Figure 6. The computer model demonstrates that with a branching ratio for R8a-ACN and R8c-ACN of 1 and 0, respectively, model predictions of AHP yields are much higher than experimental results in the high $[CH_3OH]_0$:$[acetone]_0$ ratio experiments. Predicted PAA, MHP, and CO_2 yields are much lower than the corresponding experimental values. Incorporation of reaction R8c-ACN into the model with a yield of 0.67 leads to good agreement between the model and experiments. Because of the better agreement between product yields measured by HPLC and FTIR (compared to the product yields measured from the $CH_3C(O)O_2 + HO_2$ reaction), uncertainties associated with the measured branching ratios for R8-ACN are estimated to be about 30%, lower than the uncertainties associated with the branching ratios for R8-ACT. As with R8-ACT, because of the additional radical reaction channel, the overall rate coefficient may be higher than the previously reported value.

In experiments with both methanol and acetone present, a complete carbon balance cannot be obtained for acetone oxidation because two of the expected products (formaldehyde and carbon monoxide) are also present because of the added methanol and its oxidation products. To further test our understanding of the reaction mechanism, an experiment was carried out in which ^{13}C labeled methanol was used to generate HO_2. Product yields from these experiments are given in Table 5. The carbon balance for the identified products is 91%. The remaining products, which account for 9% of the converted acetone, are expected to be hydroxyacetone and methyl glyoxal. In Acuchem simulations carried out under the appropriate experimental conditions, the predicted yields of hydroxyacetone and methyl glyoxal are 3% and 8%, respectively, which are both below the detection limits in the experiments, and which are in excellent agreement with the missing carbon balance.

Bridier et al.[33] reported data that are consistent with a branching ratio for R8a-ACN of unity (see Table 2) on the basis of kinetic simulations of flash photolysis experiments in which the concentrations of peroxy radicals were monitored by UV absorption spectroscopy. The origin of the discrepancy between this work and the results of Bridier et al. is unclear but it could indicate a problem with the UV cross sections used in that study.

A possible alternative explanation for the observed product distribution in our study is that reaction channel R8d-ACN rather than R8c-ACN is an important pathway

$$CH_3C(O)CH_2OO + HO_2 \rightarrow CH_3C(O)CHO + H_2O + O_2 \quad \text{(R8d-ACN)}$$

The resultant methylglyoxal may then react with Cl atoms to produce acetyl peroxy radicals which would then generate PAA, MHP, and CO_2 as discussed above

$$CH_3C(O)CHO + Cl\ (+ O_2) \rightarrow CH_3C(O)O_2 + CO + HCl \quad (R25)$$

To investigate this possibility, simulations were carried out in which branching ratios for R8a and R8d were set to 0.33 and 0.67, respectively (not shown). In these calculations the yields of both MHP and PAA remained constant at about 0.08 as the $[CH_3OH]_0$:[acetone]$_0$ ratio was varied from 0 to 0.5. Because the concentrations of methanol and acetone are high compared to methylglyoxal during these experiments, Cl atoms predominantly react with methanol and acetone rather than methylglyoxal. Reaction R25 is thus too slow to generate the quantities of MHP and PAA observed in the high $[CH_3OH]_0$ experiments, and reaction R8d cannot account for the observed product distributions. A significant branching ratio for R8c therefore appears to be the best available explanation for the experimental observations, although we cannot rule out a contribution from R8d-ACN.

(iv) OH Radical Formation in the $RO_2 + HO_2$ Reactions. From the discussion above, it is clear that the experimental data are consistent with high yields of OH radicals in the reaction between HO_2 and acetyl peroxy radicals and in the reaction between HO_2 and acetonyl peroxy radicals. Given that the relative rate constants for the reaction of acetone/methanol and acetaldehyde/methanol are significantly different for OH- and Cl-initiated reactions,[31] the possibility was considered that relative rate plots could be used as additional evidence for the importance of reaction R8c in the high $[CH_3OH]_0$ experiments. As the methanol concentration increases, the OH radical concentration is also expected to increase, and thus a higher fraction of methanol and the carbonyls will react with OH rather than Cl in these experiments. The slope of the relative rate plots would thus be expected to systematically change as the methanol concentration is varied (see Figure 8 in ref 16). Experimental relative rate plots do show a dependence on the methanol: acetaldehyde ratio, but it is difficult to quantitatively assign this to the occurrence of reaction 8c. This apparent discrepancy can be explained by examining the Acuchem simulations described above. In these simulations, it is apparent that OH formation from the Cl-atom-initiated oxidation of hydroperoxides (e.g., reactions R19 and 20) is a larger OH source than reaction R8c, and relative rate plots thus cannot easily be used as indirect evidence for reaction channel R8c in these experiments. For acetone, the product yields do not vary between $[CH_3OH]_0$/[acetone]$_0$ values of 0.1 and 0.5, indicating that even in the low $[CH_3OH]_0$ experiments, acetonyl peroxy radicals reacted predominantly with HO_2. The change in the slope of the relative rate plots as the methanol concentration increases is thus expected to be minimal, and the analysis could not be performed. Furthermore, the large difference in relative rates for acetone and methanol precludes an accurate measurement of this ratio.

Atmospheric Implications

As described in the Introduction, $RO_2 + HO_2$ reactions are important chain termination processes that moderate the concentrations of radical species and ozone in the lower atmosphere. In this work, evidence has been presented indicating that organic peroxy radicals containing a carbonyl group at the α-position ($CH_3C(O)O_2$) or β-position ($CH_3C(O)CH_2O_2$) do not exclusively react with HO_2 to form a hydroperoxide (R8a) and that a significant fraction of radicals are recycled in these reactions (R8c). This may lead to higher concentrations of pollutants such as OH radicals and ozone than is currently predicted by air pollution models.

To investigate the potential impact of these reactions on tropospheric ozone and OH concentrations, several simple box model simulations were carried out using the OZIPR computer program.[34] In the first set of simulations, conditions typical of a North American city during summer were chosen, and concentrations of OH and ozone were monitored as the branching ratios for reactions R8a and R8c were varied between 0 and 1. In these simulations, the branching ratios had a negligible impact on the concentrations of these secondary pollutants (typically less than 1%). In a second set of simulations, the calculations were repeated but the NO_x emission rates were reduced by a factor of 10. With all of the $RO_2 + HO_2$ reactions set to $Y_{R8c} = 1$, the peak OH radical concentration increased from 3.3×10^6 molecules cm^{-3} to 4.7×10^6 molecules cm^{-3}, while the change in the peak ozone concentration was small (<5%). Incorporating only the branching ratios measured for acetyl and acetonyl peroxy radicals into the model (and with all other $RO_2 + HO_2$ branching ratios set to $Y_{R8a} = 1$) had a much smaller impact on both ozone (<1%) and OH (<5%). This result is not surprising since oxygenated organics make up only a small fraction of total VOC emissions in these simulations.

From the simulations described here, it appears that chain propagation in $RO_2 + HO_2$ reactions (R8c) may have a small impact on tropospheric chemistry under low NO_x conditions. The impact of these reactions on OH radical concentrations will be greater for aged air, which typically contains higher concentrations of oxygenated organics and lower levels of NO_x. To predict the extent of this impact, a more detailed database of $RO_2 + HO_2$ branching ratios is needed. Finally, reaction 8 will not provide as strong an atmospheric source of acetic acid as previously thought. Further investigations of the product yields from these reactions as a function of temperature are clearly required.

Acknowledgment. The authors thank Tim Wallington and Mike Hurley for supplying spectra of peroxides. A.S.H. thanks NCAR's Atmospheric Chemistry Division for the award of a Visiting Fellowship that enabled this work to be performed. A.S.H. also thanks the donors of the Petroleum Research Fund (American Chemical Society #37996-GB6) for financial support. The National Center for Atmospheric Research is operated by the University Corporation for Atmospheric Research, under the sponsorship of the National Science Foundation. This work was supported in part by a grant from the NASA Upper Atmosphere Research Program.

References and Notes

(1) Finlayson-Pitts, B. J.; Pitts, J. N. *Chemistry of the Upper and Lower Atmosphere*; Academic Press: San Diego, CA, 2000.

(2) Atkinson, R. Gas-Phase Tropospheric Chemistry of Volatile Organic Compounds: 1. Alkanes and Alkenes. *J. Phys. Chem. Ref. Data* **1997**, *26*(2), 215.

(3) Wallington, T. J.; Japar, S. M. Reaction of $CH_3O_2 + HO_2$ in Air at 295 K: A Product Study. *Chem. Phys. Lett.* **1990**, *167*, 513−518.

(4) Wallington, T. J.; Japar, S. M. FTIR Product Study of the Reaction of $C_2H5O_2 + HO_2$ in Air at 295 K. *Chem. Phys. Lett.* **1990**, *166*, 495−499.

(5) Lightfoot, P. D.; Roussel, P.; Caralp, F.; Lesclaux, R. Flash Photolysis Study of the $CH_3O_2 + CH_3O_2$ and $CH_3O_2 + HO_2$ Reactions between 600 and 719 K: Unimolecular Decomposition of Methylhydroperoxide. *J. Chem. Soc,. Faraday Trans.* **1991**, *87*, 3213−3220.

(6) Wallington, T. J. Fourier Transform Infrared Product Study of the Reaction of $CH_3O_2 + HO_2$ over the Pressure Range 15−700 Torr at 295 K. *J. Chem. Soc., Faraday Trans.* **1991**, *87*, 2379−2382.

(7) Spittler, M.; Barnes, I.; Becker, K. H.; Wallington, T. J. Product Study of the $C_2H_5O_2 + HO_2$ Reaction in 760 Torr of Air at 284−312 K. *Chem. Phys. Lett.* **2000**, *321*, 57−61.

(8) Elrod, M. J.; Ranschaert, D. L.; Schneider, N. J. Direct Kinetics Study of the Temperature Dependence of the CH_2O Branching Channel for the $CH_3O_2 + HO_2$ Reaction. *Int. J. Chem. Kinet.* **2001**, *33*(6), 363−376.

(9) Jackson, A. V.; Hewitt, C. N. Atmospheric hydrogen peroxide and organic hydroperoxides: a review. *Crit. Rev. Env. Sci. Tech.* **1999**, *29*, 175−228.

(10) Sander, R. Compilation of Henry's Law Constants for Inorganic and Organic Species of Potential Importance in Environmental Chemistry, Version 3. http://www.mpch-mainz.mpg.de/~sander/res/henry.html (accessed 1999).

(11) Friedlander, S. K.; Yeh, E. K. The Submicron Atmospheric Aerosol as a Carrier of Reactive Chemical Species: Case of Peroxides. *Appl. Occup. Environ. Hyg.* **1998**, *13*(6), 416.

(12) Hasson, A. S.; Paulson, S. E. An Investigation of the Relationship between Gas-phase and Aerosol-borne Hydroperoxides in Urban Air. *J. Aerosol Sci.* **2003**, *34*, 459−468.

(13) Niki, H.; Maker, P. D.; Savage, C. M.; Breitenbach, L. P. FTIR Study of the Kinetics and Mechanism for Cl-Atom-Initiated Reactions of Acetaldehyde. *J. Phys. Chem.* **1985**, *89*, 588−591.

(14) Moortgat, G. K.; Veyret, B.; Lesclaux, R. Kinetics of the Reaction of HO_2 with $CH_3C(O)O_2$ in the Temperature Range 253−368 K. *Chem. Phys. Lett.* **1989**, *160*, 443−447.

(15) Horie, O.; Moortgat, G. K. Reactions of $CH_3C(O)O_2$ Radicals with CH_3O_2 and HO_2 between 263 and 333 K. *J. Chem. Soc., Faraday Trans.* **1992**, *88*, 3305−3312.

(16) Crawford, M. A.; Wallington, T. J.; Szente, J. J.; Maricq, M. M.; Francisco, J. S. Kinetics and Mechanism of the Acetylperoxy + HO_2 Reaction. *J. Phys. Chem. A* **1999**, *103*, 365−378.

(17) Tomas, A.; Villenave, E.; Lesclaux, R. Reactions of the HO_2 Radical with CH_3CHO and $CH_3C(O)O_2$ in the Gas Phase. *J. Phys. Chem. A* **2001**, *105*, 3505−3514.

(18) Orlando, J. J.; Tyndall, G. S.; Vereecken, L.; Peeters, J. The Atmospheric Chemistry of the Acetonoxy Radical. *J. Phys. Chem. A* **2000**, *104*, 11578−11588.

(19) Tyndall, G. S.; Cox, R. A.; Granier, C.; Lesclaux, R.; Moortgat, G. K.; Pilling, M. J.; Ravishankara, A. R.; Wallington, T. J. Atmospheric Chemistry of Small Peroxy Radicals. *J. Geophys. Res. D* **2001**, *106*, 12157−12182.

(20) Sulbaek-Anderson, M. P.; Hurley, M. D.; Wallington, T. J.; Ball, J. C.; Martin, J. W.; Ellis, D. A.; Mabury, S. A. Atmospheric Chemistry of C_2F_5CHO: Mechanism of the $C_2F_5C(O)O_2 + HO_2$ Reaction. *Chem. Phys. Lett.* **2003**, *381*, 14−21.

(21) Miller, C. E.; Lynton, J. I.; Keevil, D. M.; Francisco, J. S. Dissociation Pathways of Peroxyacetyl Nitrate (PAN). *J. Phys. Chem. A* **1999**, *103*, 11451−11459.

(22) Wallington, T. J.; Hurley, M. D.; Ball, J. C. FTIR Product Study of the Reaction of $CH_3OCH_2O_2 + HO_2$. *Chem. Phys. Lett.* **1993**, *211*, 41−47.

(23) Wallington, T. J.; Hurley, M. D.; Schneider, N. J.; Sehested, J.; Nielson, O. J. Mechanistic Study of the Gas-Phase Reaction of CH_2FO_2 Radicals with HO_2. *Chem. Phys. Lett.* **1994**, *218*, 34−42.

(24) Wallington, T. J.; Hurley, M. D.; Schneider, N. J. Atmospheric Chemistry of CH_3Cl: Mechanistic Study of the Reaction of CH_2ClO_2 Radicals with HO_2. *Chem. Phys. Lett.* **1996**, *251*, 164−173.

(25) Shetter, R. E.; Davidson, J. A.; Cantrell, C. A.; Calvert, J. G. *Rev. Sci. Instrum.* **1987**, *58*, 1427.

(26) Hasson, A. S.; Orzechowska, G. E.; Paulson, S. E. Production of Stabilized Criegee Intermediates and Peroxides in the Gas-Phase Ozonolysis of Alkenes: 1. Ethene, *Trans*-2-Butene and 2,3-Dimethyl-2-Butene. *J. Geophs. Res.* **2001**, *106*(D24), 34131−34142.

(27) Hasson, A. S.; Ho, A.; Kuwata, K. T.; Paulson, S. E. Production of Stabilized Criegee Intermediates and Peroxides in the Gas-Phase Ozonolysis of Alkenes: 2. Asymmetric and Biogenic Alkenes. *J. Geophys. Res.* **2001**, *106* (D24), 34143.

(28) Hartkamp, H.; P. Bachhausen. A Method for the Determination of Hydrogen Peroxide in Air. *Atmos. Environ.* **1987**, *21*(10), 2207−2213.

(29) Niki, H.; Maker, P. D.; Savage, C. M.; Breitenbach, L. P. Fourier Transform Infrared Studies of the Self-Reaction of $C_2H_5O_2$ Radicals. *J. Phys. Chem.* **1982**, *86*, 3825−3829.

(30) Wallington, T. J.; Gierczak, C. A.; Ball, J. C.; Japar, S. M. Fourier Transform Infrared Study of the Self-Reaction of $C_2H_5O_2$ Radicals in Air at 295 K. *Int. J. Chem. Kinet.* **1989**, *21*, 1077−1089.

(31) DeMore, W. B.; Sander, S. P.; Golden, D. M.; Hampson, R. F.; Kurylo, M. J.; Howard, C. J.; Ravishankara, A. R.; Kolb, C. E.; Molina, M. J. Chemical Kinetics and Photochemical Data for use in Stratospheric Modeling: Evaluation No. 11, Jet Propulsion Laboratory Publication 97-4, 1997.

(32) Braun, W.; Herron, J. T.; Kahaner, D. K. *Int. J. Chem. Kinet.* **1988**, *20*, 51.

(33) Bridier, I.; Veyret, B.; Lesclaux, R.; Jenkin, M. E. Flash Photolysis Study of the UV Spectrum and Kinetics of Reactions of the Acetonylperoxy Radical. *J. Chem. Soc., Faraday Trans.* **1993**, *89*, 2993−2997.

(34) *Ozone Isopleth Plotting Program Research Version;* Environmental Protection Agency.